Published in final edited form as:
Invest Ophthalmol Vis Sci. 2008 October ; 49(10): 4384–4391. doi:10.1167/iovs.08-1688.

Regulation by $P2X_7$: Epithelial Migration and Stromal Organization in the Cornea

Courtney Mayo[1], **Ruiyi Ren**[1], **Celeste Rich**[1], **Mary Ann Stepp**[2], and **Vickery Trinkaus-Randall**[1,3]

1*Department of Biochemistry, Boston University School of Medicine, Boston, Massachusetts*

2*Department of Anatomy and Reparative Medicine, The George Washington University, Washington, DC.*

3*Department of Ophthalmology, Boston University School of Medicine, Boston, Massachusetts*

Abstract

PURPOSE—Previously, the authors demonstrated that BzATP, a $P2X_7$ receptor agonist, enhanced corneal epithelial migration in vitro. The goal here was to characterize the role of the $P2X_7$ receptor in the repair of in vivo corneal epithelial debridement wounds and in the structural organization of the corneal stroma.

METHODS—Epithelial debridement was performed on $P2X_7$ knockout ($P2X_7^{-/-}$) and wild-type (WT) mice, and eyes were harvested after 16 hours. Corneas were stained with Richardson vital stain, and the wound area was recorded. Corneas were fixed and prepared for light microscopic, immunohistochemical, and electron microscopic analysis. Cuprolinic blue staining was performed to analyze stromal proteoglycans (PGs). Real-time PCR was performed to examine the expression of stromal collagens.

RESULTS—$P2X_7$ was present in the WT corneal epithelium but was not detected in $P2X_7^{-/-}$ mice. Pannexin-1, a protein demonstrated to interact with $P2X_7$, was absent from the wound edge in $P2X_7^{-/-}$. This was associated with a trend toward delayed corneal reepithelialization. Stromal ultrastructure and collagen alignment were altered in $P2X_7^{-/-}$, and collagen fibrils had smaller diameters with a larger interfibrillar distances. Expression of collagen alpha1(I) and alpha3(v) was reduced. There were 30% fewer sulfated PGs along fibrils in the $P2X_7^{-/-}$ stroma.

CONCLUSIONS—In the absence of the $P2X_7$ receptor, the expression of proteins in the corneal epithelium was altered and wound healing was compromised. Loss of receptor resulted in morphologic changes in the stroma, including changes in alignment of collagen fibrils, decreased expression of collagen, and smaller fibrils with fewer PGs per fibril.

Purinergic receptors have been linked to a variety of conditions within the eye. These include dry eye,[1–3] corneal epithelial migration and wound healing,[4–7] increased trabecular outflow facility,[8] and mucin secretion.[9] Injury of corneal epithelial cells in culture releases ATP and activates purinergic receptors, which induces downstream signaling events including the mobilization of Ca^{2+} and cell migration. The stimulation of purinergic receptors can occur as a result of injury, activation of stress receptors, or shear force.[4,6,10–16] These receptors are divided into two classes of different functions, the P2Y, which are G-protein–coupled receptors, and the $P2X_7$, which are ion-gated channels.

Corresponding author: Vickery Trinkaus-Randall, Department of Ophthalmology, L904, Boston University School of Medicine, 80 E. Concord Street, Boston, MA 02118; vickery@bu.edu.

Disclosure: **C. Mayo**, None; **R. Ren**, None; **C. Rich**, None; **M.A. Stepp**, None; **V. Trinkaus-Randall**, None

Previously, we showed that the stimulation of purinergic receptors, including $P2X_7$, induces the migration of corneal epithelial cells in a chemotactic migration assay.[4] However, the role of the $P2X_7$ receptor in cell-cell communication and the propagation of Ca^{2+} waves differ from those of the P2Y receptors. When Ca^{2+} imaging experiments were used to evaluate cell communication after injury, we found that injury was not attenuated by the activation of $P2X_7$ by BzATP.[4] This suggested that the receptor is not involved in the early wound response but may mediate later phases of wound repair. Our goal was to determine the role that the $P2X_7$ receptor plays in wound healing and in the organization of the corneal stroma.

The $P2X_7$ receptor has two transmembrane domains and an extended C terminus that contains a tumor necrosis factor receptor-related death domain.[17–19] Activation of the receptor with ATP or BzATP allows the mobility of Na^+, K^+, and Ca^{2+} ions. Repeated stimulation that might occur with a major wound, changes in extracellular pH, or receptor density results in the formation of a pore. Recently, it has been shown that pannexin-1 binds at the C terminus and regulates the formation of the large nonspecific pore.[20,21] Pannexins are similar to the connexins, and both form hemichannels and gap junctions between cells and mediate cell-cell communication.[22] To date, the expression of pannexins in the cornea is unknown.

$P2X_7$ is implicated in thyroid papillary cancer,[23] apoptosis of human cervical epithelial cells,[24] IL-1β release and inflammation,[25,26] and proliferation of neuroblastoma cells.[27] In addition, it has been shown to regulate bone formation and resorption, resulting in thin long bones.[28] Although the expression and localization of $P2X_7$ has been explored in the retina,[29–31] the role of $P2X_7$ in corneal wound healing and structure has yet to be investigated.

In this article, we present in vivo data demonstrating the role of $P2X_7$ in corneal epithelial wound repair and stromal architecture through the use of $P2X_7$ knockout mice ($P2X_7^{-/-}$). The results indicate, for the first time, the expression and localization of $P2X_7$ in the mouse cornea, and they show that the downregulation of $P2X_7$ delays the healing of corneal epithelial wounds. This delay is accompanied by a change in expression of proteins involved in the migration process. In addition, we found that $P2X_7$ plays a regulatory role in the structure and organization of stromal collagen in the cornea.

MATERIALS AND METHODS

Materials

$P2X_7$ knockout mice ($P2X_7^{-/-}$), strain B6.129P2-P2rx7^{tm1Gab}/J, and their wild-type (WT) counterparts, strain C57BL/6J, were obtained from Jackson Laboratories (Bar Harbor, ME) 5 weeks postnatally and were acclimated for 16 days. The antibody directed against $P2X_7$ was purchased from Lifespan Biosciences (Seattle, WA), whereas the antibody directed against $P2Y_4$ was from Chemicon (Temecula, CA). Antibodies to paxillin (pY^{118}) and FAK (pY^{397}) were from Biosource (Camarillo, CA), and the antibody against pannexin-1 was from Santa Cruz Biotechnology (Santa Cruz, CA). Anti-fade, nuclear dye (To-Pro 3AM), Alexa Fluor-conjugated secondary antibodies, reagent (TRIzol), DNaseI, random hexamers, MMLV reverse transcriptase, and RNaseH were purchased from Invitrogen (Carlsbad, CA). Cuprolinic blue and other supplies for electron microscopy were from Electron Microscopy Sciences (Hatfield, PA). RNase inhibitor and gene expression assays (TaqMan) were from Applied Biosystems (Foster City, CA). Routine chemicals were obtained from Sigma (St. Louis, MO) or American Bioanalytical (Natick, MA).

In Vivo Corneal Epithelial Debridement Wounds

All experiments were carried out in accordance with the guidelines and the approval of The George Washington University Institutional Animal Use and Care Committee and the ARVO

Statement for the Use of Animals in Ophthalmic and Vision Research. Manual debridement wounds were performed on corneas of 7-week-old mice, as described by Stepp and Zhu. [32] Briefly, mice were anesthetized with ketamine (5 mg/mL; Aveco Co., Inc., Fort Dodge, IA) and xylazine (20 mg/mL; Miles Inc., Shawnee Mission, KS). A topical anesthetic (proparacaine ophthalmic solution) was applied to the ocular surfaces until the blink sensation was absent. Corneas were scraped with a dull scalpel to remove the epithelium within a 1.5-mm central corneal area, which had been demarcated with a dull trephine. After wounding, eyes were treated with erythromycin ophthalmic ointment to minimize inflammation and to keep the ocular surface moist. Animals were humanely killed 16 hours after wounding. Corneas were immediately stained with Richardson vital stain and were photographed through a dissecting microscope. For morphologic analysis, eyes were enucleated and fixed in a 50:50 mixture of methanol and dimethyl sulfoxide for 2 hours at −20°C and were then stored in 100% methanol at −20°C. Images of 12 WT and 12 $P2X_7^{-/-}$ eyes were analyzed using NIH ImageJ software. Each wound area was measured independently by three investigators (n = 12 eyes in each group).

Microscopy

Light Microscopy—Enucleated, wounded eyes from each group were embedded in paraffin. Six-micrometer serial sections were cut and mounted on glass slides. Mounted sections were deparaffinized by two sequential 10-minute washes in xylene, followed by washes in 100%, 95%, and 70% ethanol. Sections were stained with Masson trichrome to examine collagen and stromal thickness. In addition, unwounded eyes from each group were embedded in epon/araldite, sectioned, and stained with toluidine blue.

Immunohistochemistry and Confocal Laser Microscopy—Immunohistochemistry was performed in a humidified chamber. Sections from three eyes in each group containing leading edges of the wound were blocked with 3% BSA in PBS, followed by incubation with appropriately diluted primary antibody in 1% BSA in PBS for 3 hours. Control sections were incubated with 1% BSA in PBS in place of primary antibody. Sections were washed and incubated with Alexa Fluor 488-conjugated secondary antibody for 1 hour Slides were washed three times in PBS and incubated for 15 minutes in nuclear dye (To-Pro 3AM; Invitrogen) diluted 1:1000 in PBS. Slides were washed, covered with anti-fade, and coverslipped. Sections were imaged and analyzed using a confocal microscope (LSM 510 200M; Zeiss, Thornwood, NY), as previously described.[7]

Transmission Electron Microscopy—For routine electron microscopy, four unwounded corneas were processed for transmission electron microscopy (TEM), as described in Trinkaus-Randall and Gipson. [33] Images were taken under an electron microscope (300 TM; Philips; Eindhoven, Netherlands).

Cuprolinic Blue Staining

An electron-dense reagent, cuprolinic blue, which defines the sizes and directional orientations of proteoglycan (PG) chains, was used. In other studies, it has been used to demonstrate the association between sulfated PGs and matrix molecules such as collagen.[34] Two eyes in each group were stained with 0.2% cuprolinic blue (in buffer containing 0.3 M $MgCl_2$) for 24 hours[35] and were dehydrated and processed for TEM, as described previously.

Real-Time PCR

Corneas were removed from unwounded eyes, and epithelium was scraped off. Corneal stromas were homogenized in reagent (TRIzol; Invitrogen), and RNA was extracted according to manufacturer's guidelines. Genomic DNA was removed by incubation with DNaseI in the

presence of 1 U/μL RNase inhibitor. RNA was annealed with random hexamer primers, and first-strand cDNA synthesis was carried out with M-MLV reverse transcriptase. Negative controls were performed without the reverse transcriptase. The resultant cDNA was treated with RNaseH. Real-time PCR was performed (ABI 7300; Applied Biosystems). Gene expression assays (TaqMan; Invitrogen) used were Mm00489842_m1 for alpha3(v), Rn00801649_g1 for alpha(1)I, and eukaryotic 18S rRNA endogenous control. Cycling parameters were as follows: 50°C for 2 minutes, 95°C for 10 minutes, 45 cycles of 95°C for 15 seconds, and 60°C for 1 minute Results are presented as relative expression normalized to 18s rRNA and were calculated using the ΔΔCt method.

Statistical Analysis

For epithelial wounds, three independent investigators scored the wounds, the results were averaged and expressed as ± SEM, and Student's *t*-test was performed. For stromal collagen, measurements of collagen fibril size and interfibrillar distance and size and number of proteoglycans were made using the Universal Desktop Ruler application. Results were averaged and expressed as ± SEM, and Student's *t*-test was performed.

RESULTS

Corneas from $P2X_7^{-/-}$ and WT mice were examined, and the epithelium and stroma were compared. Mature corneas appeared grossly normal and had no apparent opacity. There were no differences in weight between the two groups and no detectable abnormalities in mobility or skin. This is the first report demonstrating a role for $P2X_7$ in corneal wound healing and stromal ultrastructure.

Epithelial Wound Healing

Epithelial debridement wounds measuring 1.5 mm in diameter were made, and wound closure was evaluated after 16 hours in WT and $P2X_7^{-/-}$ animals. Visual evaluation and photography were performed after topical administration of Richardson stain. Wounds were measured by three independent investigators. There was a trend toward delayed wound closure for the $P2X_7^{-/-}$ mice (Table 1).

Cross-sections of the epithelial debridements of WT and $P2X_7^{-/-}$ corneas were stained with Masson trichrome 16 hours after injury. Anterior sections of the cornea demonstrated that the region adjacent to the wound edge in the $P2X_7^{-/-}$ was fragile, and the epithelium was routinely separated from the anterior stroma rather than along the basal lamina (Fig. 1A, arrow). Separation may be attributed to loose collagen fibrils in unwounded corneas. In addition, the stroma of the $P2X_7^{-/-}$ was thicker than that of the WT, possibly because of the spaces in the mid and posterior cornea (Fig. 1B).

Immunohistochemical staining was performed, and the localization of proteins was visualized using confocal microscopy. Tissue sections were costained with nuclear dye (nuclear dye [To-Pro 3AM; Invitrogen]; see Materials and Methods). The absence of the receptor was verified in the $P2X_7^{-/-}$ mice corneas using an antibody directed against the $P2X_7$ receptor. As predicted, $P2X_7$ was present in the cornea of the WT mice (Fig. 2). To determine whether $P2Y_4$ receptors, shown to have a role in in vitro cell migration, were modulated by the $P2X_7$ receptor, we examined its localization in $P2X_7^{-/-}$ and WT. The $P2Y_4$ receptor was detected along the apical epithelium in the WT, but in the $P2X_7^{-/-}$, $P2Y_4$ appeared diffuse throughout the apical and basal cells. Pannexin-1 was examined because it has been shown to interact with the $P2X_7$ receptor and form nonspecific pores.[20,21] In WT and $P2X_7^{-/-}$, pannexin-1 was localized to punctate regions between cells distal to the leading edge (defined as 105 μm back from the leading edge (Fig. 2, inset). However, it was only detected at the leading edge in the

WT. Use of appropriate rabbit or goat secondary antibodies alone showed negligible staining (Fig. 2).

Because wound healing was compromised in the $P2X_7^{-/-}$ animals, we examined proteins (paxillin and FAK) known to be associated with cell migration. The localization of phosphorylated (p) paxillin differed between WT and $P2X_7^{-/-}$. Phosphorylated paxillin was diffuse throughout the epithelium in WT and $P2X_7^{-/-}$ animals. However, intense staining was found distal to the leading edge along the epithelial stromal interface in the WT (Fig. 2, inset). In addition, p-paxillin was more prominent in WT than $P2X_7^{-/-}$ when quantified with the Zeiss image analysis program (data not shown). There were no detectable differences in phosphorylated focal adhesion kinase (p-FAK) between $P2X_7^{-/-}$ and WT epithelium. This was consistent at the leading edge and distal from the wound. Sections stained only with secondary antibody were negligible (Fig. 2).

The epithelial basal lamina region was examined at the electron microscopic level, and hemidesmosomal structures and anterior collagen were examined. Filaments projected through the lamina lucida, and electron-dense regions of intermediate filaments splayed into the cytoplasm in WT and $P2X_7^{-/-}$ corneas (Fig. 3). Although anchoring fibrils are not prominent in mice, they were detected in WT and $P2X_7^{-/-}$. No morphologic change was observed in either the basal lamina or Descemet membrane of the $P2X_7^{-/-}$ animals (data not shown).

Stromal Ultrastructure and Regulation of Collagen

The ultrastructure of the unwounded, central stroma was examined and divided into anterior, middle, and posterior regions. Orthogonal and perpendicular lamellae in the $P2X_7^{-/-}$ corneal stromas were thicker and fewer than in the WT. A typical $P2X_7^{-/-}$ stroma revealed orthogonal and perpendicular lamellae with an average thickness of 1259 ± 100 nm, whereas WT averaged 770 ± 56 nm (Fig. 4). Collagen in the $P2X_7^{-/-}$ stromas lacked the orthogonal organization typical of the WT. For example, in the $P2X_7^{-/-}$, the collagen fibrils within an array were not aligned in a parallel pattern, and there was a paucity of collagen fibrils in cross-section (Fig. 4A, Fig. 5B). Instead of the prototypical parallel lamellae, the fibrils were present in a swirling configuration (Figs. 5A, 5B). Electron microscopic images indicated that the difference was greater in the mid and posterior parts of the cornea.

Collagen fibril diameter and interfibrillar distance were determined for each region of the stroma. The average fibril diameter in $P2X_7^{-/-}$ mice was smaller in all regions of the stroma than in WT mice. Although fibril diameter steadily increased from the anterior to the posterior stroma in WT, that of the $P2X_7^{-/-}$ remained consistent over all regions (Fig. 6). There was a significant difference between WT and $P2X_7^{-/-}$ in average fibril diameter over all regions ($P \leq 0.0001$; data not shown). The change in collagen fibril diameter was accompanied by a change in packing of lamellae. Distributions of the interfibrillar distances of various regions were examined (Fig. 7A). There was a wide range in $P2X_7^{-/-}$ and WT corneas, with the greatest differences in the posterior region. In all the regions examined, the interfibrillar distance was greater in $P2X_7^{-/-}$ mice than in WT mice. The difference in interfibrillar distance was significant over all regions (Fig. 7B). Although the mean interfibrillar distances in corneas of both mouse strains increased from anterior to posterior, the trend was more pronounced in $P2X_7^{-/-}$ mice.

Real-time PCR was performed on corneal stromas and a number of other tissues (tail, lung, aorta) to examine collagen expression levels. In the stromas, the mRNA expression of both collagen types, alpha1(I) and alpha3(v), was reduced by greater than 75% (Fig. 8). Interestingly, though the expression of alpha(1)I was reduced in the $P2X_7^{-/-}$ stroma, it was increased by more than twofold in the aorta (data not shown), indicating that the regulation was tissue specific.

We examined whether a change in sulfated PG was associated with the change in collagen organization. Corneas were incubated in cuprolinic blue, which binds sulfated moieties, before processing for TEM. Three distinct populations of electron-dense proteoglycans were observed in WT and $P2X_7^{-/-}$. These included filaments regularly associated with collagen fibrils, elongated filaments that run along the fibrils, and filaments seen in cross-section (Fig. 9A). This arrangement of PG filaments supported that previously described in WT mice.[36] In the WT stroma, the electron-dense filaments were present along the collagen fibril, with a PG to fibril ratio of 9.06 ± 0.63 PG/μm. In contrast, in $P2X_7^{-/-}$, the ratio of sulfated PGs detected along collagen fibrils was 6.07 ± 0.60 PGs/μm (Fig. 9B).

DISCUSSION

The $P2X_7$ receptor is an ATP-gated ion channel thought to be associated with a number of proteins, including pannexin-1. It has a large cytoplasmic domain, and the structurally important regions have been studied through the examination of a number of mutant receptors.[16,18,19,37,38] Previous studies report that $P2X_7^{-/-}$ mice have lower bone mineral content with reduced periosteal bone formation and hypothesize that the receptor is required for proper skeletal response to mechanical loading.[28,39] This is the first study that examines the role of $P2X_7$ in the cornea. We found that it mediates not only the organization and expression of stromal collagen but also the expression of proteins involved in wound repair.

We demonstrated in $P2X_7^{-/-}$ mice that there was a downward trend in the rate of epithelial wound repair. The change in rate may be associated with the morphology of the leading edge. In the WT, the epithelium directly behind the leading edge consists of two to three cell layers, whereas in the $P2X_7^{-/-}$, it remained a single cell layer for a longer distance. At the same time, the leading edge of the $P2X_7^{-/-}$ was more fragile, and tearing was observed along the stroma. These morphologic differences may be attributed to changes in protein expression at the leading edge.

Paxillin is involved in migration and is known to be phosphorylated in wounded and migratory cells.[40–42] Phosphorylated paxillin was diffusely localized in all layers of the epithelium in $P2X_7^{-/-}$ and WT. However, in the WT, there was additional localization of p-paxillin in a margin at the epithelial-stromal interface that was not observed in the $P2X_7^{-/-}$. This agreed with previous in vitro studies in which the stimulation of corneal epithelial cells with nucleotides induced the phosphorylation of paxillin.[7,43] Our current results suggest that $P2X_7$ has a role in the nucleotide-induced phosphorylation of paxillin.

Recently, investigators have shown that $P2X_7$ associates with pannexin-1 to form a large, nonspecific pore.[20,21] Although pannexin-1 can couple, and form an active pore, with $P2X_7$, it has other functions independent of $P2X_7$, such as the formation of hemichannels. We do not understand how the pannexin was regulated, but we detected its presence, which was altered compared with WT. Our results show that pannexin-1 was not localized at the leading edge of the wound in $P2X_7^{-/-}$ mice but that it was detected 105 μm from the leading edge in distinct areas between the cells. In WT mice, it was found at the leading edge and throughout the epithelium.

Loose collagen fibrils were detected under the epithelial wound edge of the $P2X_7^{-/-}$ animals; therefore, we examined the epithelial-basal lamina interface and the stroma. Although we detected no difference in the hemidesmosomal region, we observed a change in the regulation and the organization of the stroma. The stromal matrix is composed primarily of collagen fibrils stacked in orderly lamellae surrounded by PGs. This organization of PGs and collagen fibrils is thought to be responsible for the optical and structural features of the stroma.[44–46] It is possible that the change in stromal organization in the $P2X_7^{-/-}$ results from reduced collagen

expression because we found that the expression of collagens alpha1(I) and alpha3(V) mRNA was reduced in $P2X_7^{-/-}$ mice at 4 weeks of age (Fig. 8). However, it is unknown whether the expression is decreased throughout development. Additionally, collagen fibrils in $P2X_7^{-/-}$ stromas demonstrated an increased interfibrillar distance (Fig. 7) that would result in a reduction in the number of collagen fibrils within a given area. This reduced packing could result in the disorganization observed. Interestingly, an increased interfibrillar distance is detected at specific developmental time points in the lumican KO mouse,[47] suggesting that $P2X_7^{-/-}$ mice may develop at a different rate than their age-matched WT counterparts. In other studies, a thin stroma was observed in collagen V mutations where the stromal thickness was decreased over the entire cornea. This was accompanied by an overall decrease in fibril density.[48] In the type V collagen mutations, the orthogonal arrays were maintained, but in the $P2X_7^{-/-}$, the orthogonal arrays of collagen were fewer and thicker than those in the WT stroma. In addition, there were irregularities throughout the stroma with collagen fibrils that appeared to swirl in the posterior cornea. The mechanisms underlying these changes are not understood, and studies to examine epithelial-mesenchymal interactions such as those described by Hay[49] are under way.

The structural basis for corneal transparency requires a homogeneous distribution of collagen fibrils, fibril packing, and arrangement of orderly orthogonal arrays. It was surprising, then, that the $P2X_7^{-/-}$ mouse corneas were transparent. It is possible that the change in fibril size was offset by the increase in interfibrillar spacing and the decrease in sulfated PGs. For example, transparency is retained in Ehlers-Danlos syndrome, in mice with type V collagen mutations,[48] and in mucopolysaccaridosis III,[50] where there is a difference in diameter accompanied by a retention in packing. Some investigators have shown a lack of association between central corneal thickness and refraction, whereas others have detected differences in the central corneal thickness among myopic, hyperopic, and emmetropic eyes.[51,52]

The irregularity in spacing of the collagen fibrils observed in the $P2X_7^{-/-}$ mice may be indicative of changes in glycosaminoglycans (GAGs).[53] When the stroma is compromised because of disease or injury, biochemical and structural changes occur. In general, after injury, collagen fibrils have larger diameters accompanied by irregular interfibrillar spacing, thought to be caused in part by a change in the expression of sulfated GAGs.[54–56] The size and number of PGs has been demonstrated in the literature to indicate phases of development or injury.[55,57] Further analysis of the stroma with cuprolinic blue staining revealed sulfated PGs, with fewer PG chains in $P2X_7^{-/-}$ detected along collagen fibrils. In fact, Young[36] has provided an important study on mice GAGs for the explicit purpose of comparing WT with KO. They report that GAGs found in mice were detected as filaments associated with the collagen fibrils or as long, thick filaments that run along and traverse the fibrils. Although $P2X_7^{-/-}$ mice had fewer GAG chains than WT, both groups exhibited the overall structures described by Young.[36] Future studies will determine the expression of specific PGs and examine how mice with irregular collagen and fewer PGs respond to and repair stromal injuries.

These studies show for the first time that the $P2X_7$ receptor plays a critical role in the corneal epithelium and stroma. The results indicate that $P2X_7$ is necessary for timely healing of abrasion wounds and normal stromal collagen structure. Our current findings indicate that the $P2X_7$ receptor plays a critical role in the formation of a properly organized stroma. Because $P2X_7$ may contribute to the regulation of a number of proteins, future studies will examine whether the decrease in migration is related to changes in epithelial-mesenchymal interactions and whether the changes in stromal architecture depend on changes in collagen regulation, as demonstrated by the type V mutation.[48]

Acknowledgments

The authors thank Haiyan Gong and Matthew Nugent for their discussions of the manuscript, and Rozanne Richman for technical expertise.

Supported by National Institutes of Health/National Eye Institute Grants EY06000 (VT-R.) and EY008512 (MAS) and by Massachusetts Lions Eye Research (VT-R).

References

1. Tauber J, Davitt WF, Bokosky JE, et al. Double-masked, placebo-controlled safety and efficacy trial of diquafosol tetrasodium (INS365) ophthalmic solution for the treatment of dry eye. Cornea 2004;23:784–792. [PubMed: 15502479]
2. Fujihara T, Murakami T, Nagano T, Nakamura M, Nakata K. INS365 suppresses loss of corneal epithelial integrity by secretion of mucin-like glycoprotein in a rabbit short-term dry eye model. J Ocul Pharmacol Ther 2002;18:363–370. [PubMed: 12222766]
3. Fujihara T, Murakami T, Fujita H, Nakamura M, Nakata K. Improvement of corneal barrier function by the P2Y2 agonist INS365 in a rat dry eye model. Invest Ophthalmol Vis Sci 2001;42:96–100. [PubMed: 11133853]
4. Weinger I, Klepeis V, Trinkaus-Randall V. Tri-nucleotide receptors play a critical role in epithelial cell wound repair. Purinergic Signalling 2005;1:281–292. [PubMed: 18404512]
5. Pintor J, Bautista A, Carracedo G, Peral A. UTP and diadenosine tetraphosphate accelerate wound healing in the rabbit cornea. Ophthalmic Physiol Opt 2004;24:186–193. [PubMed: 15130167]
6. Mediero A, Peral A, Pintor J. Dual roles of diadenosine polyphosphates in corneal epithelial cell migration. Invest Ophthalmol Vis Sci 2006;47:4500–4506. [PubMed: 17003445]
7. Klepeis VE, Weinger I, Kaczmarek E, Trinkaus-Randall V. P2Y receptors play a critical role in epithelial cell communication and migration. J Cell Biochem 2004;93:1115–1133. [PubMed: 15449317]
8. Soto D, Pintor J, Peral A, Gual A, Gasull X. Effects of dinucleoside polyphosphates on trabecular meshwork cells and aqueous humor outflow facility. J Pharmacol Exp Ther 2005;314:1042–1051. [PubMed: 15947035]
9. Jumblatt JE, Jumblatt MM. Regulation of ocular mucin secretion by $P2Y_2$ nucleotide receptors in rabbit and human conjunctiva. Exp Eye Res 1998;67:341. [PubMed: 9778415]
10. Khakh BS, North AR. P2X receptors as cell-surface ATP sensors in health and disease. Nature 2006;442:527. [PubMed: 16885977]
11. Yang L, Cranson D, Trinkaus-Randall V. Cellular injury induces activation of MAPK via P2Y receptors. J Cell Biochem 2004;91:938–950. [PubMed: 15034929]
12. Klepeis VE, Cornell-Bell A, Trinkaus-Randall V. Growth factors but not gap junctions play a role in injury-induced Ca^{2+} waves in epithelial cells. J Cell Sci 2001;114:4185–4195. [PubMed: 11739651]
13. Neary JT, Kang Y, Willoughby KA, Ellis EF. Activation of extracellular signal-regulated kinase by stretch-induced injury in astrocytes involves extracellular ATP and P2 purinergic receptors. J Neurosci 2003;23:2348–2356. [PubMed: 12657694]
14. Boucher I, Yang L, Mayo C, Klepeis V, Trinkaus-Randall V. Injury and nucleotides induce phosphorylation of epidermal growth factor receptor: MMP and HB-EGF dependent pathway. Exp Eye Res 2007;85:130. [PubMed: 17490650]
15. Lazarowski ER, Homolya L, Boucher RC, Harden TK. Direct demonstration of mechanically induced release of cellular UTP and its implication for uridine nucleotide receptor activation. J Biol Chem 1997;272:24348–24354. [PubMed: 9305892]
16. Cheewatrakoolpong B, Gilchrest H, Anthes JC, Greenfeder S. Identification and characterization of splice variants of the human $P2X_7$ ATP channel. Biochem Biophys Res Commun 2005;332:17. [PubMed: 15896293]
17. Surprenant A, Rassendren F, Kawashima E, North RA, Buell G. The cytolytic P_{2z} receptor for extracellular ATP identified as a P_{2x} receptor ($P2X_7$). Science 1996;272:735–728. [PubMed: 8614837]

18. Adriouch S, Dox C, Welge V, Seman M, Koch-Nolte F, Haag F. Cutting edge: A natural P451L mutation in the cytoplasmic domain impairs the function of the mouse $P2X_7$ receptor. J Immunol 2002;169:4108–4112. [PubMed: 12370338]
19. Smart ML, Gu B, Panchal RG, et al. $P2X_7$ receptor cell surface expression and cytolytic pore formation are regulated by a distal C-terminal region. J Biol Chem 2003;278:8853–8860. [PubMed: 12496266]
20. Pelegrin P, Surprenant A. Pannexin-1 mediates large pore formation and interleukin-1β release by the ATP-gated $P2X_7$ receptor. EMBO J 2006;25:5071–5082. [PubMed: 17036048]
21. Locovei S, Scemes E, Qiu F, Spray DC, Dahl G. Pannexin1 is part of the pore forming unit of the $P2X_7$ receptor death complex. FEBS Lett 2007;581:483. [PubMed: 17240370]
22. Vanden Abeele F, Bidaux G, Gordienko D, et al. Functional implications of calcium permeability of the channel formed by pannexin 1. J Cell Biol 2006;174:535–546. [PubMed: 16908669]
23. Solini A, Cuccato S, Ferrari D, et al. Increased $P2X_7$ receptor expression and function in thyroid papillary cancer: a new potential marker of the disease? Endocrinology 2008;149:389–396. [PubMed: 17947359]
24. Wang Q, Wang L, Feng YH, Li X, Zeng R, Gorodeski GI. $P2X_7$ receptor-mediated apoptosis of human cervical epithelial cells. Am J Physiol Cell Physiol 2004;287:C1349–C1358. [PubMed: 15269006]
25. Lister M, Sharkey J, Sawatzky DA, et al. The role of the purinergic $P2X_7$ receptor in inflammation. J Inflamm (Lond) 2007;4:5. [PubMed: 17367517]
26. Ferrari D, et al. The $P2X_7$ receptor: a key player in IL-1 processing and release. J Immunol 2006;176:3877–3883. [PubMed: 16547218]
27. Raffaghello L, Chiozzi P, Falzoni S, Di Virgilio F, Pistoia V. The $P2X_7$ receptor sustains the growth of human neuroblastoma cells through a substance P-dependent mechanism. Cancer Res 2006;66:907–914. [PubMed: 16424024]
28. Ke HZ, Qi H, Weidema AF, et al. Deletion of the $P2X_7$ nucleotide receptor reveals its regulatory roles in bone formation and resorption. Mol Endocrinol 2003;17:1356–1367. [PubMed: 12677010]
29. Ishii K, Kaneda M, Li H, Rockland KS, Hashikawa T. Neuronspecific distribution of $P2X_7$ purinergic receptors in the monkey retina. J Comp Neurol 2003;459:267–277. [PubMed: 12655509]
30. Puthussery T, Fletcher EL. Synaptic localization of $P2X_7$ receptors in the rat retina. J Comp Neurol 2004;472:13–23. [PubMed: 15024749]
31. Pannicke T, Fischer W, Biedermann B, et al. $P2X_7$ receptors in Muller glial cells from the human retina. J Neurosci 2000;20:5965–5972. [PubMed: 10934244]
32. Stepp MA, Zhu L. Upregulation of α9 integrin and tenascin during epithelial regeneration after debridement in the cornea. J Histochem Cytochem 1997;45:189–202. [PubMed: 9016309]
33. Trinkaus-Randall V, Gipson IK. Role of calcium and calmodulin in hemidesmosome formation in vitro. J Cell Biol 1984;98:1565–1571. [PubMed: 6715411]
34. Scott JE, Haigh M. Identification of specific binding sites for keratin sulphate proteoglycans and chondroitin-dermatan sulphate proteoglycans on collagen fibrils in cornea by the use of cupromeronic blue in “critical-electrolyte-concentration” techniques. Biochem J 1988;253:607–610. [PubMed: 2972275]
35. Gong H, Freddo TF, Johnson M. Age-related changes of sulfated proteoglycans in the normal human trabecular meshwork. Exp Eye Res 1992;55:691. [PubMed: 1478279]
36. Young RD, Tudor D, Hayes AJ, et al. Atypical composition and ultrastructure of proteoglycans in the mouse corneal stroma. Invest Ophthalmol Vis Sci 2005;46:1973–1978. [PubMed: 15914611]
37. Gu BJ, Sluyter R, Skarratt KK, et al. An Arg307 to Gln polymorphism within the ATP-binding site causes loss of function of the human $P2X_7$ receptor. J Biol Chem 2004;279:31287–31295. [PubMed: 15123679]
38. Feng YH, Li X, Wang L, Zhou L, Gorodeski G. I: a truncated $P2X_7$ receptor variant ($P2X_7$-j) endogenously expressed in cervical cancer cells antagonizes the full-length P2X7 receptor through heterooligomerization. J Biol Chem 2006;281:17228–17237. [PubMed: 16624800]
39. Li J, Liu D, Ke HZ, Duncan RL, Turner CH. The $P2X_7$ nucleotide receptor mediates skeletal mechanotransduction. J Biol Chem 2005;280:42952–42959. [PubMed: 16269410]

40. Kimura K, Hattori A, Usui Y, et al. Stimulation of corneal epithelial migration by a synthetic peptide (PHSRN) corresponding to the second cell-binding site of fibronectin. Invest Ophthalmol Vis Sci 2007;48:1110–1118. [PubMed: 17325153]
41. Zaidel-Bar R, Milo R, Kam Z, Geiger B. A paxillin tyrosine phosphorylation switch regulates the assembly and form of cell-matrix adhesions. J Cell Sci 2007;120:137–148. [PubMed: 17164291]
42. Petit V, Boyer B, Lentz D, Turner CE, Thiery JP, Vallés AM. Phosphorylation of tyrosine residues 31 and 118 on paxillin regulates cell migration through an association with CRK in NBT-II cells. J Cell Biol 2000;148:957–970. [PubMed: 10704446]
43. Trinkaus-Randall V, Kewalramani R, Payne J, Cornell-Bell A. Calcium signaling induced by adhesion mediates protein tyrosine phosphorylation and is independent of pHi. J Cell Physiol 2000;184:385–399. [PubMed: 10911371]
44. Farrell, R. Corneal transparency. In: Albert, D.; Jacobiec, SA., editors. Principles and Practice of Ophthalmology. Philadelphia: WB Saunders; 1994. p. 64-81.
45. Maurice DM. The structure and transparency of the cornea. J Physiol 1957;136:263–286. [PubMed: 13429485]
46. Trinkaus-Randall, V. Cornea. In: Lanza, R., editor. Principles of Tissue Engineering. Austin, TX: R.G. Landes Company; 1997. p. 383-402.
47. Beecher N, Chakravarti S, Joyce S, Meek KM, Quantock AJ. Neonatal development of the corneal stroma in wild-type and lumicannull mice. Invest Ophthalmol Vis Sci 2006;47:146–150. [PubMed: 16384956]
48. Segev F, Héon E, Cole WG, et al. Structural abnormalities of the cornea and lid resulting from collagen V mutations. Invest Ophthalmol Vis Sci 2006;47:565–573. [PubMed: 16431952]
49. Hay ED. The mesenchymal cell, its role in the embryo, and the remarkable signaling mechanisms that create it. Dev Dyn 2005;233:706–720. [PubMed: 15937929]
50. Alroy J, Haskins M, Birk DE. Altered corneal stromal matrix organization is associated with mucopolysaccharidosis I, III and VI. Exp Eye Res 1999;68:523. [PubMed: 10328965]
51. Sanchis-Gimeno J, Lleo-Perez A, Alonso L, Rahhal MS, Martinez-Soriano F. Anatomic study of the corneal thickness of young emmetropic subjects. Cornea 2004;23:669–673. [PubMed: 15448491]
52. Cosar CB, Sener AB, Sen N, Coskunseven E. The efficacy of hourly prophylactic steroids in diffuse lamellar keratitis epidemic. Ophthalmologica 2004;218:318. [PubMed: 15334012]
53. Hassell JR, Newsome DA, Hascall VC. Characterization and biosynthesis of proteoglycans of corneal stroma from rhesus monkey. J Biol Chem 1979;254:12346–12354. [PubMed: 115885]
54. Cintron C, Hassinger LC, Kublin CL, Cannon DJ. Biochemical and ultrastructural changes in collagen during corneal wound healing. J Ultrastruct Res 1978;65:13–22. [PubMed: 722838]
55. Cintron C, Covington HI, Kublin CL. Morphologic analyses of proteoglycans in rabbit corneal scars. Invest Ophthalmol Vis Sci 1990;31:1789–1798. [PubMed: 2120145]
56. Hassell JR, Cintron C, Kublin C, Newsome DA. Proteoglycan changes during restoration of transparency in corneal scars. Arch Biochem Biophys 1983;222:362–369. [PubMed: 6847191]
57. Cintron C, Gregory JD, Damle SP, Kublin CL. Biochemical analyses of proteoglycans in rabbit corneal scars. Invest Ophthalmol Vis Sci 1990;31:1975–1981. [PubMed: 2210993]

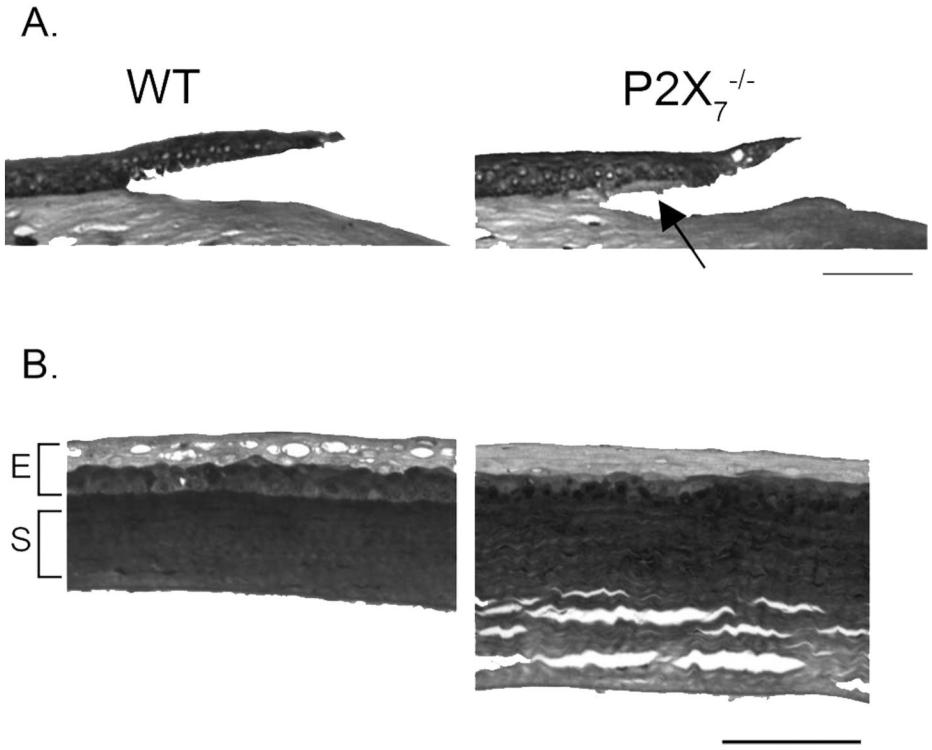

FIGURE 1.

(**A**) Light micrographs of Masson trichrome-stained corneas 16 hours after injury. *Arrow*: separation in the anterior stroma at $P2X_7^{-/-}$ wound edge. Images are representative of 12 corneas in each group. (**B**) Light micrographs of unwounded corneas. Scale bar, 75 μm for each image.

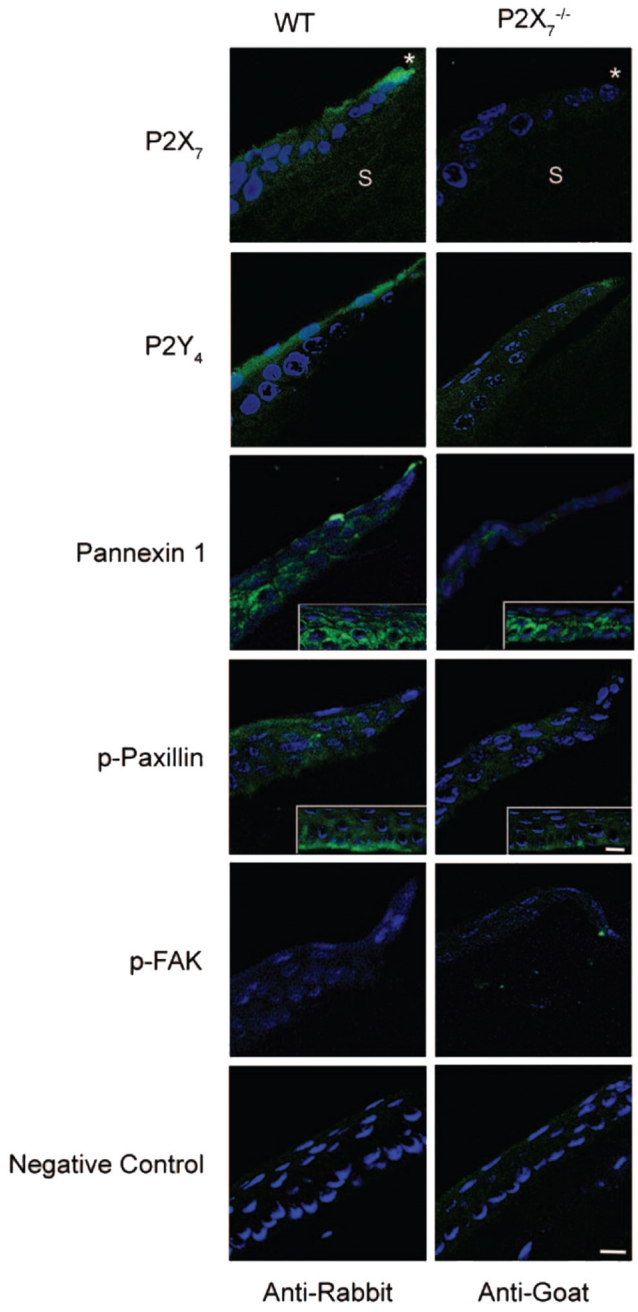

FIGURE 2.

Immunohistochemistry of proteins localized to the wound margin. Representative images from paraffin sections were probed with antibodies specific for $P2X_7$, $P2Y_4$, pannexin-1, p-paxillin, and p-FAK, followed by FITC-conjugated IgG. Nuclei were counterstained with nuclear dye (To-Pro 3AM; Invitrogen) and pseudocolored *blue*. *Asterisk*: leading edge of wound. S: stroma. Pannexin 1 (*inset*): 105 μm distal to leading edge shows punctate localization in $P2X_7^{-/-}$. p-Paxillin (*inset*): 2 × zoom, 105 μm distal to leading edge, shows localization along epithelial-stromal border in WT. Negative controls represent areas distal to the wound, probed only with secondary antibody and counterstained with nuclear dye. Scale bar, 10 μm. Images are representative of three experiments.

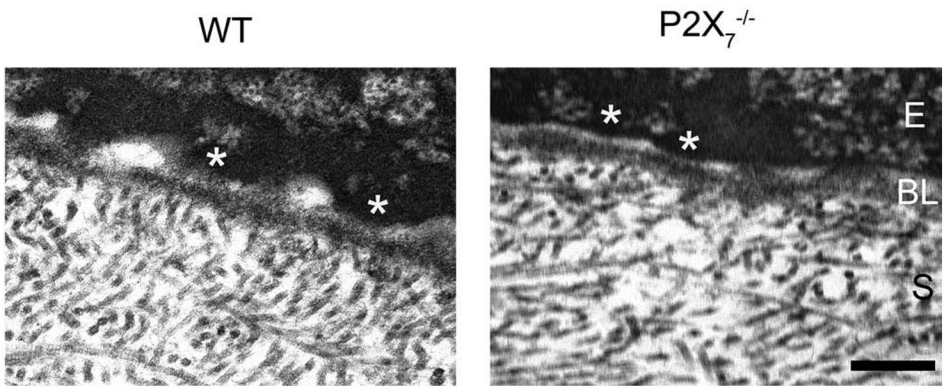

FIGURE 3.

Electron micrographs of hemidesmosomes and anterior stroma. Hemidesmosomes and anterior stromal collagen organization were evaluated distal to the wound edge. *Asterisk*: hemidesmosomal complexes. E, epithelium; BL, basal lamina; S, stroma. Micrographs are representative of at least three animals. Scale bar, 250 nm.

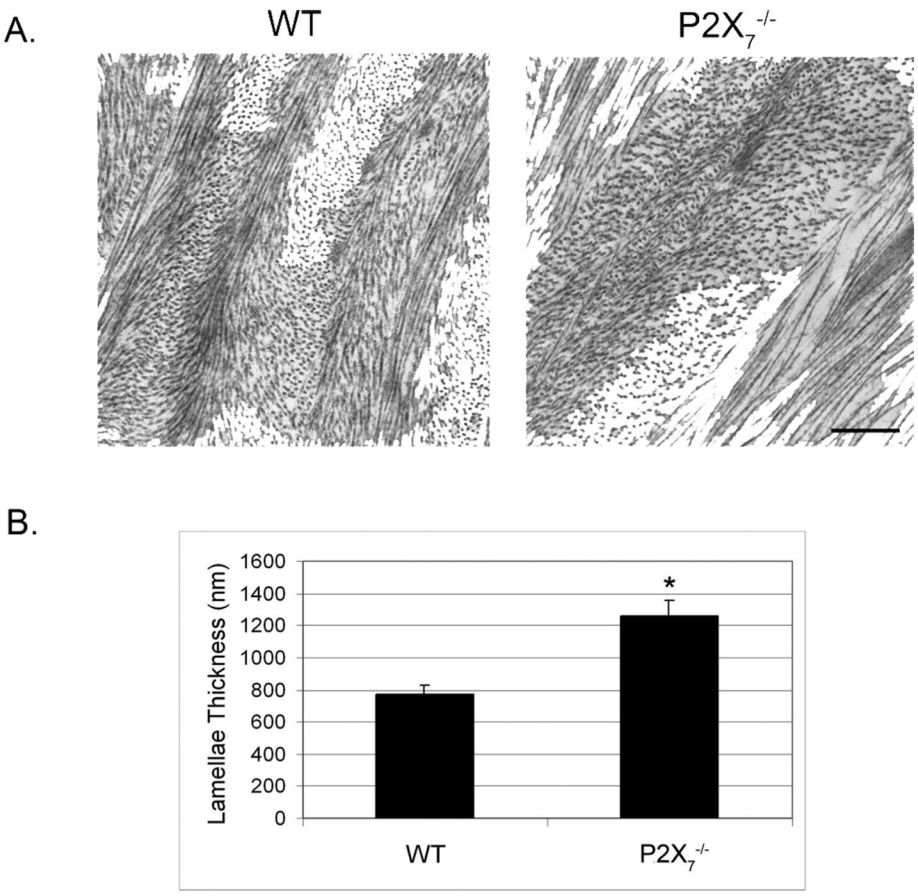

FIGURE 4.

Electron micrographs of collagen lamellae from WT and $P2X_7^{-/-}$ mice. (**A**) Lamellae are more numerous in WT than $P2X_7^{-/-}$ in the middle of the central stroma. Scale bar, 500 nm. (**B**) Mean lamellae thickness. A minimum of 34 orthogonal and perpendicular lamellae throughout the stroma were measured for each group. Data are presented as ± SEM. *$P < 0.001$; *t*-test.

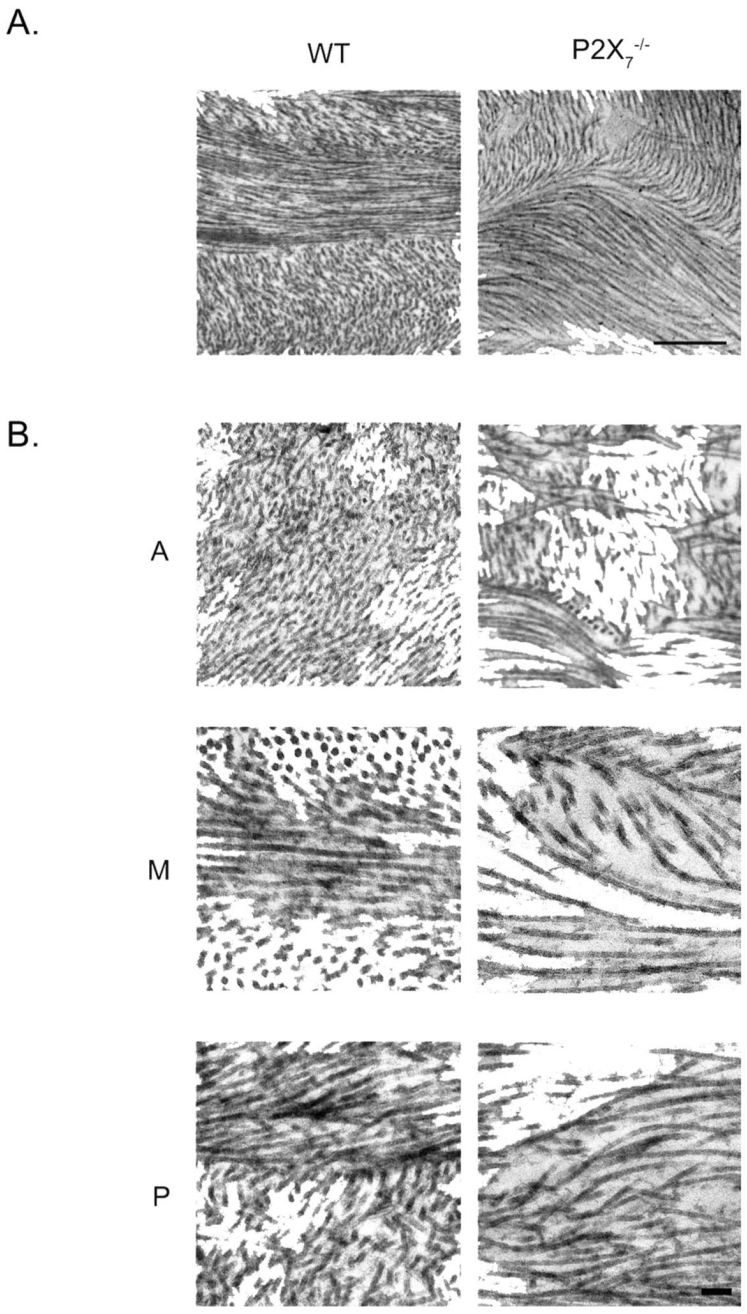

FIGURE 5.

Electron micrographs of central stromal collagen from unwounded WT and $P2X_7^{-/-}$ mice. (**A**) Low magnification of middle stroma depicts swirling of fibrils in $P2X_7^{-/-}$. (**B**) Higher magnification of three distinct regions. A, anterior; M, middle; P, posterior. Scale bar: (**A**) 500 nm; (**B**) 100 nm.

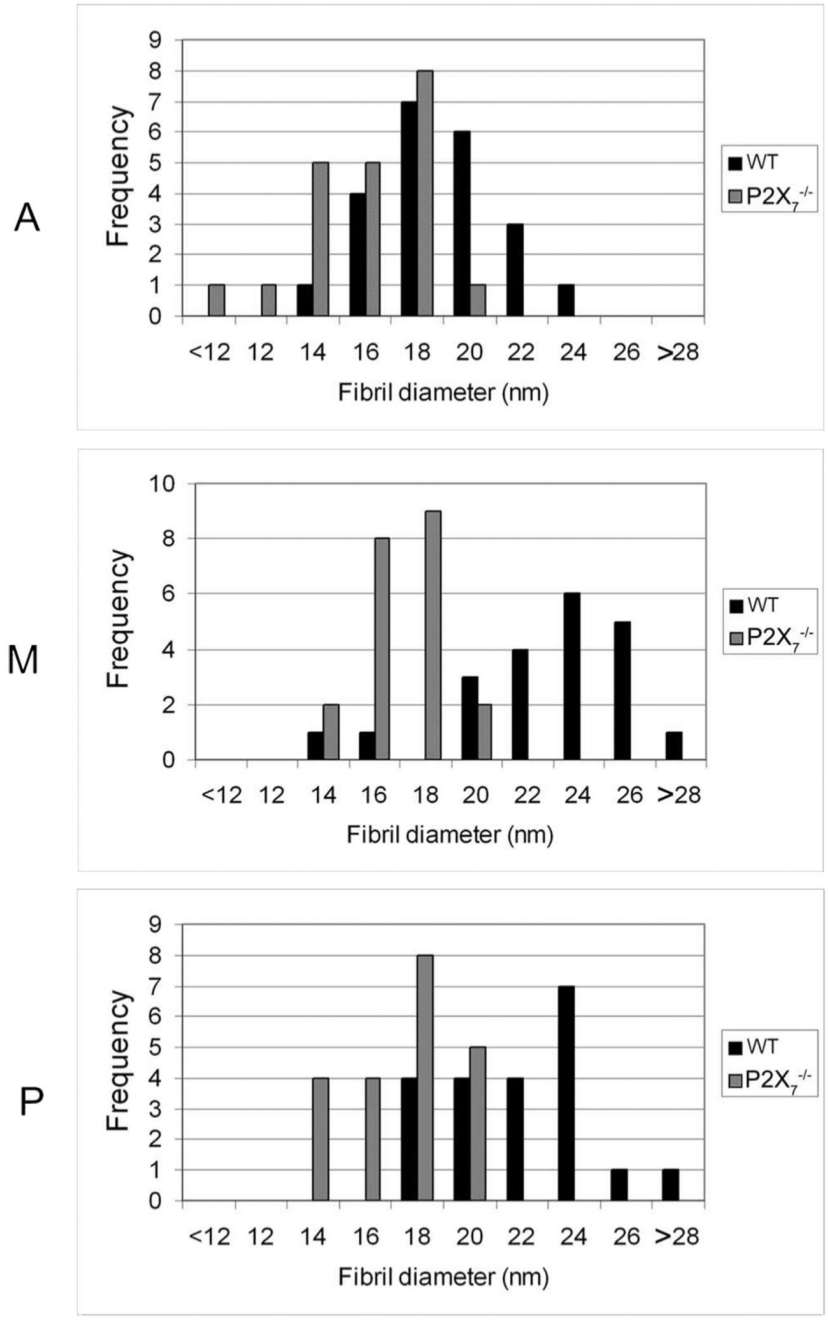

FIGURE 6.

Distribution of collagen fibril diameter in unwounded WT and $P2X_7^{-/-}$ stromas. Fibril diameter was measured and averaged for each nonoverlapping region of the stroma. A, anterior; M, middle; P, posterior. At least 21 fibrils were counted in each region.

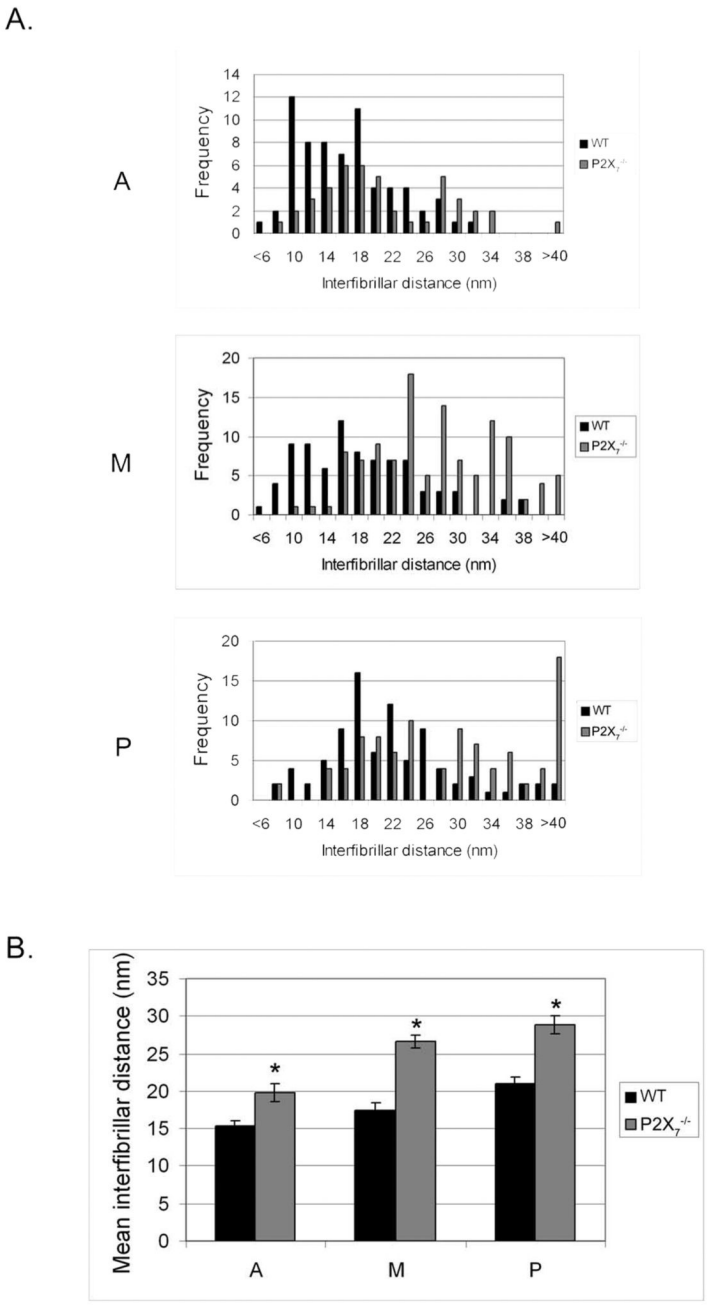

FIGURE 7.

Interfibrillar distance in unwounded WT and $P2X_7^{-/-}$ stromas. Interfibrillar distance in each nonoverlapping region was measured. (**A**) Frequency of interfibrillar distance. (**B**) Mean ± SEM interfibrillar distance of each region is graphed. A, anterior; M, middle; P, posterior. At least 40 measurements were performed for each group. **P* < 0.001; *t*-test.

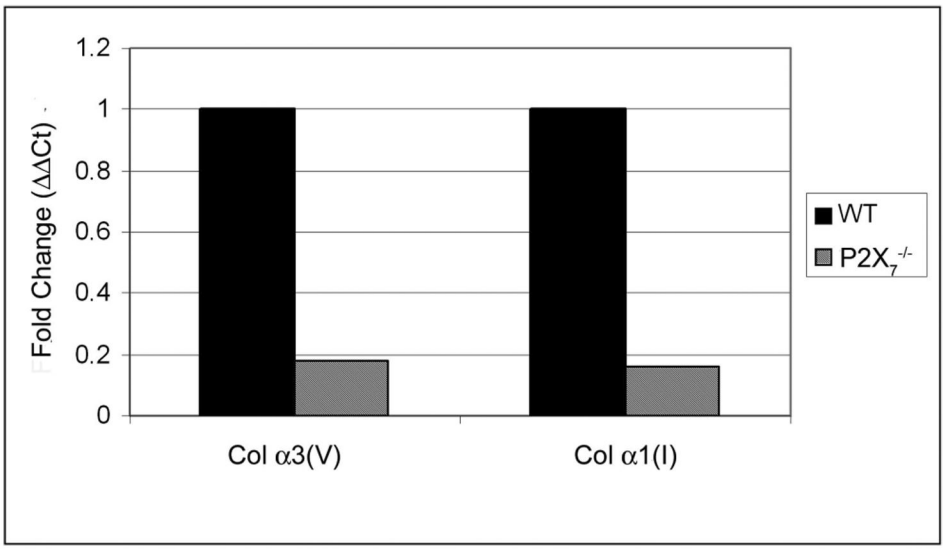

FIGURE 8.

Expression of collagen is decreased in $P2X_7^{-/-}$ unwounded stromas. Negative controls were performed minus the reverse transcriptase. Results are presented as relative expression normalized to 18s rRNA and were calculated using the ΔΔCt method.

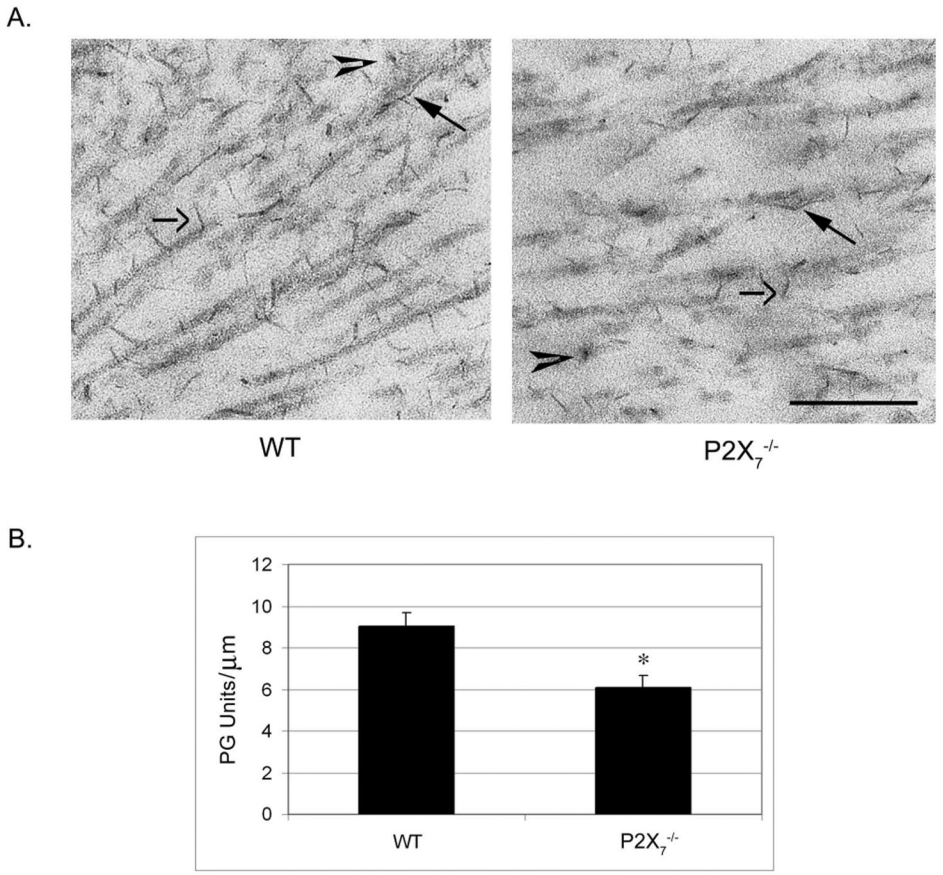

FIGURE 9.

Electron micrographs of unwounded, central stromas stained with cuprolinic blue. Tissue was stained with cuprolinic blue before it was processed for electron microscopy. (**A**) Micrographs of middle stroma. *Closed arrows*: PGs associated with collagen fibrils. *Open arrows*: elongated filaments running along fibrils. *Arrowheads*: elongated filaments seen in cross-section. Scale bar, 250 nm. (**B**) PU/collagen fibril ratio in WT and $P2X_7^{-/-}$ stromas. The length of collagen fibrils was measured, and the number of PG units along that length was counted. PG per micrometer is graphed ± SEM. At last 22 measurements were performed for each group. **P* < 0.001; *t*-test.

TABLE 1

Measurements of Wound Area in WT and $P2X_7^{-/-}$ Corneas

	WT (mm^2)	$P2X_7^{-/-}$ (mm^2)
Mean	0.47	0.64
Range	0.23–0.75	0.33–1.3
SEM	0.06	0.10

Corneal epithelial debridement was performed on the central cornea. Wound area was measured by three investigators using images taken 16 hours after wounding.